A&A 423, 221–233 (2004)
DOI: 10.1051/0004-6361:20040241

Astronomy & Astrophysics

A search for disks around exoplanet host stars

C. Saffe⋆ and M. Gómez

Observatorio Astronómico de Córdoba, Laprida 854, 5000 Córdoba, Argentina
e-mail: [saffe;mercedes]@oac.uncor.edu

Received 10 February 2004 / Accepted 4 May 2004

Abstract. We have assembled a database which comprises optical and infrared (IR) photometry of Exoplanet Host stars (EHs), and constructed the spectral energy distributions (SEDs) of these stars. We use several quantities to explore the existence of excess IR emission with respect to the photospheric level. In particular, the criteria proposed by Mannings & Barlow (1998) identify IR excess in 19–23% of the class V EH sources (i.e., in 6-7 out of 31). Several searches for Vega-like systems have yielded a similar fraction of objects with IR excess emission among main sequence stars. This excess emission is likely due to the presence of dust in circumstellar disks. We compare the optical polarization properties of the EHs, Vega-like candidate objects and pre-main sequence stars. While the median polarizations of the EHs and Vega-like candidate objects are very similar, both groups have significant lower median optical polarization values than T Tauri and Herbig AeBe stars.

Key words. stars: circumstellar matter – stars: planetary systems – technique: photometry – technique: polarimetry – stars: planetary systems: formation

1. Introduction

Doppler measurements of solar-type stars have revealed radial velocity variations interpreted as due to companions of planetary masses (see, for example, Marcy & Butler 1996; Noyes et al. 1997; Butler et al. 1996; Vogt et al. 2000). These planetary companions exhibit both circular and eccentric orbits, consistent with a formation in dissipative dusty circumstellar disks followed by gravitational perturbations (see Lin et al. 1996; Levison et al. 1998; Golderich & Sari 2003). As a group the Exoplanet Host stars (EHs) have ages of ~ 3–4×10^9 yr (Reid 2002) and spectral types G and K, reflecting the bias of high precision radial velocity measurements towards solar type stars.

IRAS data (Aumann et al. 1984) and other recently more infrared (IR) surveys (see, for example, Backman & Paresce 1993; Mannings & Barlow 1998; Sylvester & Mannings 2000; Fajardo-Acosta et al. 2000) have detected IR excess emission above the photospheric levels associated with many main sequence stars. Dusty circumstellar disks are usually invoked to explain the observed excess emission. These stars, known as the Vega-like group, have ages $\sim 10^9$ yr (Song et al. 2000, 2001) and spectral types A and F. No significant age difference seems to exist between the Vega-like and the EH groups, although the uncertainties in this parameter are usually large.

Recent studies have tried to find evidence for the presence of dusty disks associated with the EHs. In particular five stars (HD 17051, HD 210277, ϵ Eri, ρ CrB, and 55 Cnc) have been searched. In spite of the announcements of disks associated with these objects, the only clear detection so far corresponds to ϵ Eri (Greaves et al. 1998; Zuckerman 2001).

In this contribution, we present a search for disks associated with EHs based on the corresponding spectral energy distributions (SEDs). In particular, we compare the observed and the photospheric fluxes at 12 and 25 μm as well as the observed and stellar luminosities of these objects. We find several new candidate stars with IR excess emission among the EHs. We caution, however, that in most of the cases we are using IRAS upper limits for the fluxes at wavelengths longer than 12 μm, thus higher sensitivity and better resolution observations are required to confirm our candidate sources.

The sample is described in Sect. 2 and the data compilation in Sect. 3. We use the $K_s - [12]$ vs. $J - K_s$ and the $K_s - [25]$ vs. $J - K_s$ color–color diagrams to verify the presence of 12 and 25 μm excesses in the EH sample in Sect. 4. The SEDs for these sources are constructed in Sect. 5. In Sect. 6 we apply different methods to search for the IR excess emission, first employed to select Vega-like objects. The optical polarimetry properties of the EHs and Vega-like objects are compared with those of pre-main sequence stars (T Tauri and Herbig AeBe) in Sect. 7. We summarize and discuss our results in Sect. 8.

2. The sample

We derived our sample from the California and Carnegie Planet Search[1] and the Geneva Observatory Planet Search[2] lists of EHs. These objects have been found by Doppler spectroscopy and have companions with masses such that $M \sin i < 17\ M_{\rm Jup}$.

⋆ On a fellowship from CONICET, Argentina.

[1] http://exoplanets.org
[2] http://obswww.unige.ch/~udry/planet/planet.html

Table 1. Photometric catalogs used for the EHs.

Catalog	Reference	Bands	Comment
Hipparcos	ESA 1997, ESA SP-1200	B, V, I	Limiting mag V = 12.4
Tycho	ESA 1997, ESA SP-1200	B, V	Limiting mag V = 11.5
2MASS	Cutri et al. (2003)	J, H, K_s	Sources brighter than 1 mJy, $S/N > 10$
DENIS	DENIS Consortium (2003)	J, K_s, Gunn-I	Limiting mags: 18.5, 16.5, 14 respec.
MSX5C	Egan et al. (1999)	$B1$(4.29 μm), $B2$(4.25 μm) A(8.28 μm), C(12.13 μm) D(14.65 μm), E(21.34 μm)	Sensitivity of 0.1 Jy at 8.3 μm
IRAS PSC	Beichman et al. (1986)	12, 25, 60, 100 μm	Complete to 0.4, 0.5, 0.6, 1.0 Jy respec.
IRAS FSC	Moshir et al. (1989)	12, 25, 60, 100 μm	Complete to 0.2, 0.2, 0.2, 1.0 Jy respec.
ISO	Kessler (1996)	3.6, 12, 15, 20, 25, 60, 90 μm	

The EH group reflects the observational focus on near-solar-type stars where G dwarfs contribute to the majority of the detections. So far, Gl 876 is the only M dwarf known to have a planetary-mass companion. These stars have parallaxes in the range 12–311 mas (i.e., distances between 12–83 pc) and include a significant number of evolved stars with at least 10 or 11 objects in the sub-giant branch (Reid 2002). From a total of 98 EHs, we have selected a sub-sample of 61 objects for which optical and IR photometry are available to construct the SEDs.

Table 2. EHs with high proper motion and uncertain optical/IRAS source association.

Star	μ_α [mas/yr]	μ_δ [mas/yr]	r [arcsec]
HD 39091	+311.97	+1050.19	133.66
HD 89744	−120.17	−138.60	93.01
GJ 86	+2092.84	+654.32	76.62
ρ CrB	−196.89	−773.01	154.16
70 Vir	−234.81	−576.19	68.88

3. Data compilation

3.1. The photometry

Table 1 lists the catalogs used to compile the optical and the IR photometry. The Hipparcos and Tycho databases were employed to obtain the optical photometry, whereas the 2MASS and DENIS surveys provided the near-IR bands. The MSX5C, IRAS, and ISO satellites gave mid and far-IR data.

We used the calibration of Bessel (1979) for the *UBVRI* bands and that of Bessel & Brett (1988) for the *JHKLL'M* data to transform the corresponding magnitudes to flux units ([W/m^2]) when required. In the case of the 2MASS J, H, K_s magnitudes and the DENIS J, K_s, Gunn-I data, we applied the calibrations of Cohen et al. (2003) and Fouqué et al. (2000), respectively. A color-correction factor was introduced into the IRAS fluxes (Beichman et al. 1986), assuming a roughly 5000 K black-body photospheric SED for the stars in our sample.

3.2. Positional associations

We have cross-correlated the different catalogs examining the positional associations of each object. High proper motions are usually the main cause of discrepancies. The largest differences are found for the IRAS positions. Table 2 lists stars for which we find significant differences between the IRAS and Hipparcos positions. Those values are very similar to the differences obtained between the IRAS and the GSC (Guide Star Catalog) positions. The proper motions and the coordinate differences, r (in arcsec), refer to the equinox and epoch 2000.0. For these objects the optical-IR associations are uncertain.

We used the DSS (Digitized Sky Survey) plates and the GSC catalog to search for contaminating objects within the IRAS uncertainty ellipse. Only in the case of 70 Vir did we find an object (GJ 9446) within the IRAS ellipse and practically coinciding with the position of 70 Vir.

4. The K_s – [12] vs. J – K_s and the K_s – [25] vs. J – K_s diagrams

We have compiled JHK_s 2MASS and IRAS FSC data for the EH sample and constructed the $K_s - [12]$ vs. $J - K_s$ and the $K_s - [25]$ vs. $J - K_s$ color–color diagrams in Fig. 1. The circles indicate class V stars and the squares evolved (i.e., class IV/III) objects. We have eliminated 55 Cnc from the analyzed sample as the 12, 25 μm excesses and remaining IRAS fluxes are probably due to unresolved background sources (Jayawardhana et al. 2002).

The presence of dusty circumstellar material around giant stars is difficult to sustain and it may be interstellar rather than circumstellar at least in some cases (Kalas et al. 2002). Jura (1999), however, suggested that dusty circumstellar disks around giant stars may result from the destruction of comet-like objects in a Kuiper-Belt-like region as the central star ages and increases its luminosity, evolving towards the giant branch. In this paper we choose to analyse the class V and the more evolved central objects separately, although the same algorithms are applied to both groups.

We notice a homogeneous mixture of class V and evolved EHs in Fig. 1, indicating similar IR excess properties for both groups. In addition, the 12 μm excesses have a relatively smaller dispersion than the 25 μm excesses for both groups. The class V and the more evolved star samples have median $K_s - [12]$ colors of 0.38 and 0.44, respectively. For the $K_s - [25]$ colors, we obtain medians of 1.26 and 1.20, class V and evolved stars.

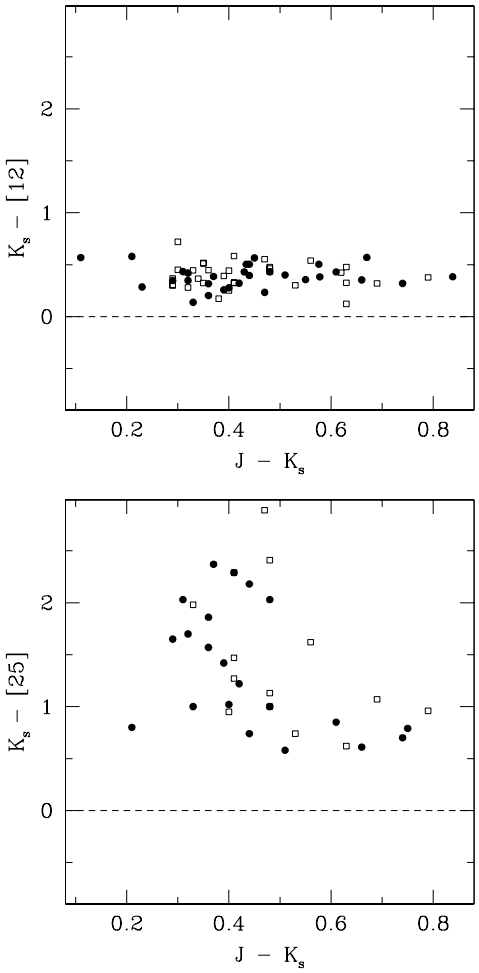

Fig. 1. $K_s - [12]$ vs. $J - K_s$ and $K_s - [25]$ vs. $J - K_s$ color–color diagrams for the sample of EHs. Luminosity class V objects are represented by circles, evolved objects by open squares. The dashed lines indicate $K_s - [12] = 0$ and $K_s - [25] = 0$, corresponding to normal main sequence stars lacking circumstellar dust.

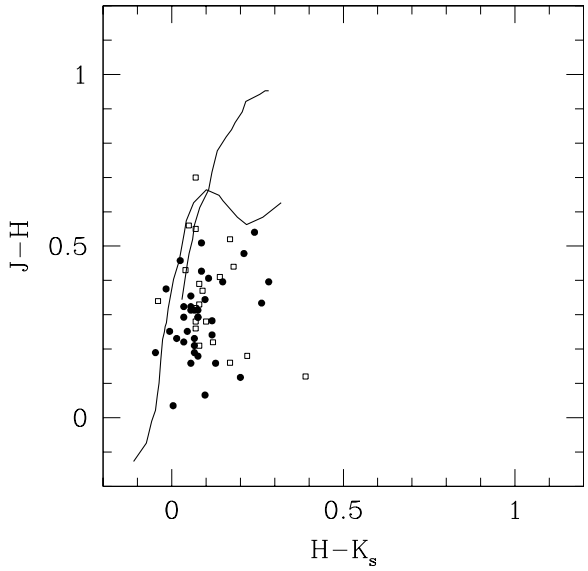

Fig. 2. $J - H$ vs. $H - K_s$ color–color diagram for the sample of EHs. Luminosity class V objects are represented by circles, evolved objects by open squares. The solid lines indicate the locations of the main and giant sequences from Bessel & Brett (1988), transformed to the 2MASS photometric system. The object with the largest $H - K_s$ is HD 216437.

Fajardo-Acosta et al. (2000) used the $K_s - [12]$ vs. $J - K_s$ diagram to select stars with 12 μm excess as Vega-like candidates. Normal main sequence stars analyzed by these authors have $K_s - [12] \sim 0$, while for stars with 12 μm excess in their sample they derived $K_s - [12] \sim 0.5$.

Herbig AeBe stars from the catalog of Thé et al. (1994) have a median $K_s - [12]$ of 4.21. Classical T Tauri stars (CTTs) and Weak emission T Tauri stars (WTTs) in the Taurus Auriga molecular cloud have median 12 μm excesses of 4.07 and 2.47, respectively (Kenyon & Hartmann 1995). Mid-infrared color excesses associated with young ($\sim$1–10 $\times$ 10^6 yr) stars are larger than those derived for the EH and the Vega-like samples (ages $\sim$1–10 $\times$ 10^8 yr). However, these objects still have significant excesses in relation to the normal main sequence stars believed to be essentially devoid of circumstellar dust.

5. The spectral energy distributions

We derived the reddening $E(B - V)$ towards each star from the observed $(B - V)$ color and intrinsic color, $(B - V)_o$, taken from the calibration of Schmidt-Kaler (1982). For the class V EHs, we typically obtained $E(B-V) \lesssim 0.03$, indicating that these objects do not have significant interstellar reddening. For the evolved objects we also derived reddening similar to the class V stars, except for some cases with negative values. We attribute these negative reddenings to errors in the observed colors, uncertainties in the spectral types or/and luminosity classes. We neglect the reddening correction in view of the very modest values obtained.

We combined optical and near-IR photometry and constructed the spectral energy distributions for the 61 EHs in our sample. We adopted the Planck function corresponding to the effective temperature of the central star to represent the photospheric contribution and normalized this black-body distribution to the optical and near-IR observed fluxes for each star.

The choice of this particular normalization impedes our detecting excesses at optical and near-infrared wavelengths. However, no significant excesses in the 1–2 μm region are expected as the EH group follows or lies relatively close to the location of the main and giant sequences in the $K_s - H$ vs. $J - K_s$ plot (see Fig. 2).

Spectral types and luminosity classes for the analyzed objects were obtained from the Hipparcos catalog as well as from Reid (2002). We adopted effective temperatures from the literature (see, for example, Chen et al. 2002; Allende Prieto & Lambert 1999). When only the spectral type and luminosity class were available we used the Schmidt-Kaler (1982) calibration to derive the $T_{\rm eff}$.

The black-body model reproduces the observed spectral distributions between 0.43 and 12 μm quite satisfactorily for most of the objects. However, most of the stars in our sample show IR excess emission at $\lambda \gtrsim 12$ μm that cannot be fitted by a single black-body model and thus cannot be attributed to

the photospheric contribution. We divide our sample of 61 EHs into two sub-sets: 31 class V and 19 class III/IV objects, the rest of the stars (11, in total) are sources of unknown luminosity class. Figure 3 shows the SEDs for a *representative* sub-sample of the class V stars with IR excess emission above the photospheric level. Figure 4 corresponds to the evolved and unknown luminosity class objects.

6. Vega-like star IR-excess-emission criteria

To better quantify the existence of excess emission above the photospheric level in the EHs we applied three criteria previously used in surveys of circumstellar dust around nearby stars. These studies basically used the following parameters: 1) $F_{12,\rm obs}/F_{12,*}$ and $F_{25,\rm obs}/F_{25,*}$, the ratios of the observed to the photospheric fluxes at 12 and 25 μm, respectively (Sylvester & Mannings 2000; Laureijs et al. 2002); 2) $L_{\rm IR}/L_*$, the fractional dusty disk luminosity (Sylvester et al. 1996); and 3) $R_{12/25}$ and $R_{25/60}$, the density flux ratios (Mannings & Barlow 1998) in combination with a positional association criterion and IRAS data quality constraints.

6.1. The ratios of the observed to the photospheric fluxes at 12 and 25 μm

We applied a spline fitting to the observed fluxes to reproduce the spectral energy distribution of each source. The black-body model atmosphere of the corresponding $T_{\rm eff}$, normalized to the optical/near-IR fluxes, was chosen to represent the photospheric continuum. We determined the ratios $F_{12,\rm obs}/F_{12,*}$ and $F_{25,\rm obs}/F_{25,*}$ and listed the corresponding values in Table 3.

Some of these objects have far-IR photometry from different sources, for instance ISO as well as IRAS PSC and IRAS FSC data are available. In these cases, we compute and list in Table 3 the $F_{25,\rm obs}/F_{25,*}$ values derived from the different surveys. In general, the $F_{25,\rm obs}/F_{25,*}$ values obtained from the ISO data are less than the same ratios derived from the IRAS fluxes. The most extreme cases are τ Boo and 47 UMa (0.98, 1.66 for τ Boo and 0.96, 1.39 for 47 UMa, ISO and IRAS bands, respectively). These stars are variable or suspected variables.

Figure 5 shows the distributions of the ratios of the observed to the photospheric fluxes at 12 and 25 μm (upper and lower panels). The continuous line indicates the class V EH subsample and the dotted line the class IV/III stars. The median of the 12 μm distributions is 1.67 for both groups. For the 25 μm data we obtain median values of 2.11 and 2.06, for the class V and evolved objects respectively.

The group of EHs has excess emission at both 12 and 25 μm. The 12 μm excess distributions of both subsamples are narrower than the 25 μm excess histograms, indicating quasi-uniform disk characteristics at 12 μm and a greater diversity of properties at 25 μm (see also Fig. 1). The Kolmogorov-Smirnov (KS) statistical test (Press et al. 1992) indicates high probabilities of the two distributions being identical. We derive probabilities of ~49% and of ~86% for the 12 and 25 μm excess distributions, for the class V and evolved objects, respectively.

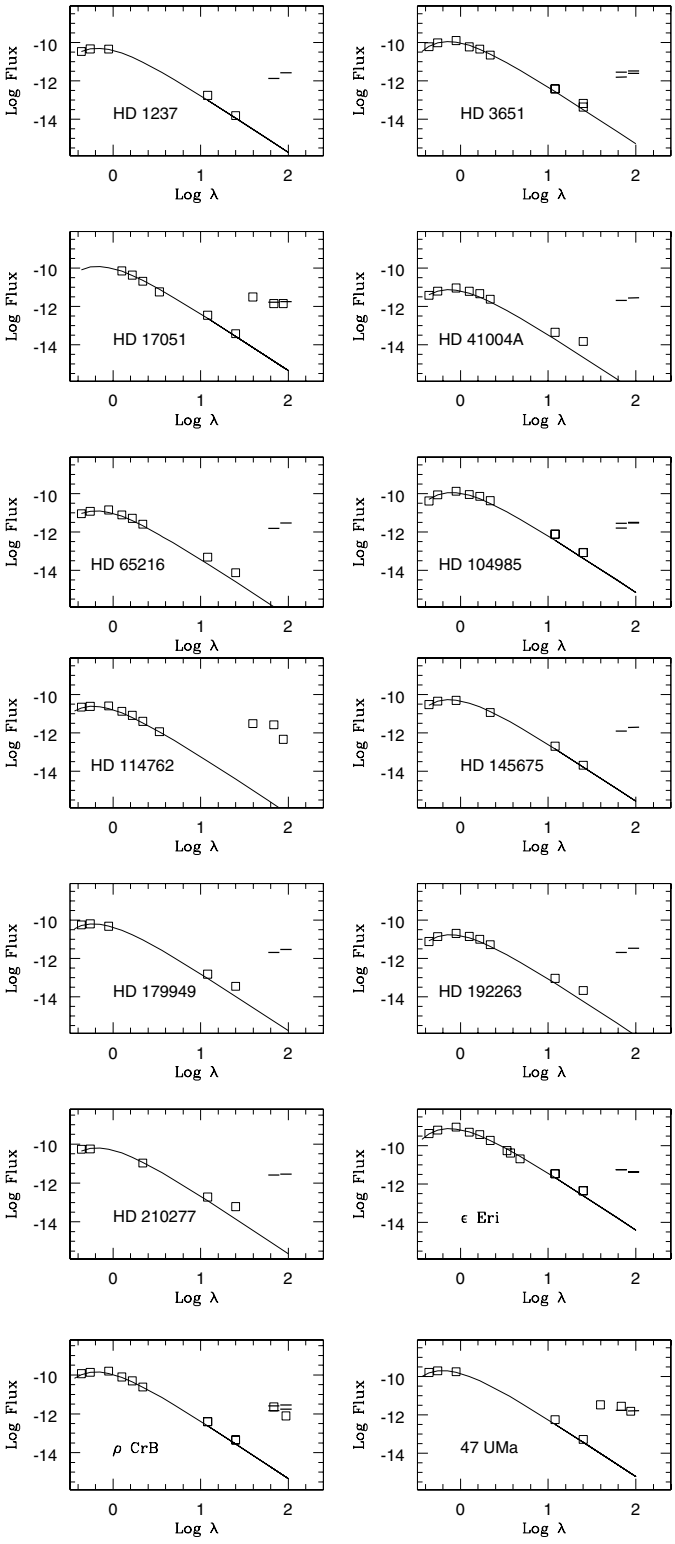

Fig. 3. SEDs for a representative sample of the class V EHs with IR excess emission. Units of flux and wavelength are W/m^2 and μm, respectively. The continuous lines represent the normalized black-body model for the appropriate $T_{\rm eff}$. The squares are the observed fluxes and the short lines correspond to the IRAS upper limits.

In Fig. 6 we plot the ratios of the observed to the photospheric fluxes at 12 and 25 μm vs. the differences between the optical and IRAS positions in arcsec. We find no clear trend

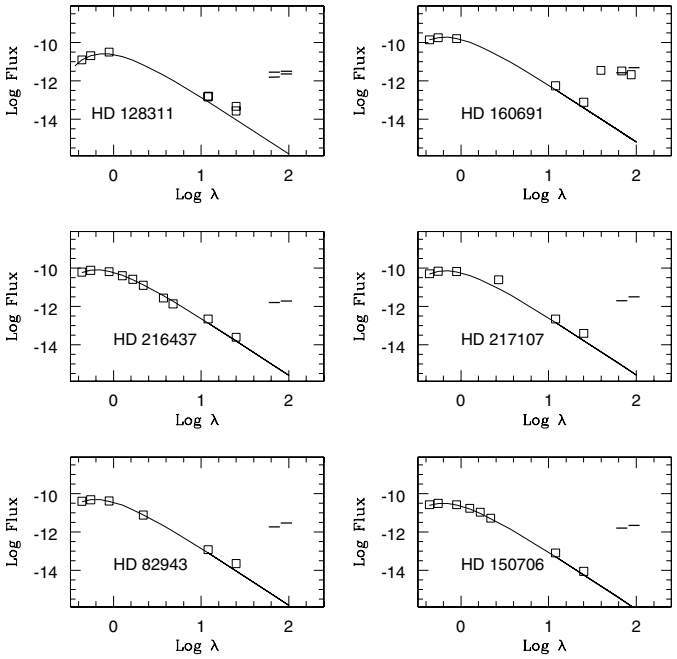

Fig. 4. SEDs for a representative sample of the evolved (HD 128311, HD 160691, HD 216437, and HD 217107) and the unknown luminosity class (HD 82943 and HD 150706) EHs having IR excess emission. Units of flux and wavelength are W/m^2 and μm, respectively. The continuous lines represent the normalized black-body model for the appropriate $T_{\rm eff}$. The squares are the observed fluxes and the short lines correspond to the IRAS upper limits.

in these plots. The 12 and 25 μm excesses do not seem to correlate with the separation. This suggests that the detected excesses are circumstellar. A positive correlation would have cast some doubts on the true circumstellar nature of the detected excesses and hinted at an interstellar origin (see Sylvester & Mannings 2000). We notice, however, that the excess emission at both wavelengths are not large and thus any faint interstellar contribution may contaminate the IRAS fluxes. In Sect. 6.3. we will apply a quality constrain to the IRAS data to better discriminate the EHs with likely far-infrared excesses.

6.2. The fractional dusty disk luminosity

Following Sylvester et al. (1996), for each target we determine $\lambda_{\rm exc}$, the wavelength where the fitted curve representing the observed spectral energy distribution and the black-body model diverge. This point marks the minimum wavelength where the excess emission begins. For most of the objects in our sample $\lambda_{\rm exc}$ = 12 μm (see Table 3).

In Vega-like stars this separation usually occurs also at 12 μm (Sylvester et al. 2001), indicating that these objects are devoid of significant amounts of hot dust in their disks and that there is little dust very close to the star. Direct imaging of some Vega-like systems (see, for example, HR 4796A and HD 141569, Augereau et al. 1999; Weinberger et al. 1999; Schneider et al. 1999) shows that the disks indeed have extensive clear inner regions, which are substantially free of dust. On the other hand, younger objects of about the same spectral types as the Vega-like stars, the Herbig AeBe stars, tend to show significant near IR excess emission (e.g., Malfait et al. 1998).

For the EHs, we have derived the stellar luminosity, L_*, integrating the black-body model over the complete wavelength range, and the observed luminosity, $L_{\rm obs}$, integrating over the fitted spline curve. To calculate the excess IR luminosity, $L_{\rm IR}$, we have subtracted the stellar (L_*) from the observed ($L_{\rm obs}$) luminosity. Table 3 gives the fractional dusty disk luminosity, $L_{\rm IR}/L_*$, the excess over the stellar luminosity.

In addition, Table 3 provides references to the catalogs used to compute the fractional luminosity, an IRAS data quality flag, and a source variability indication. The IRAS flux density measurements are flagged by *FQUAL* as either high quality, moderate quality or upper limit (*FQUAL* = 3, 2, and 1, respectively) in each band. Usually only the 12 and 25 μm bands have high or moderate quality in the sample of EHs. The IRAS data also provide a cirrus flag. The rest of the photometric catalogs used include notes indicating different factors (such as variability or multiplicity) that may affect the quality of the photometry. We have combined this information and used the Kholopov et al. (1998) catalog, *A Combined General Catalog of Variable Stars*, to include a note on the variability of the sources (see Table 3, last column). Some of the sources are variable or suspected variables and/or suffer from confusion or contamination problems.

We caution, however, that the fractional luminosity for most of the objects in Table 3 has been derived using IRAS upper limits, particularly at 100 μm. In Sect. 6.3. we will apply the criteria of Mannings & Barlow (1998) and put constraints on the IRAS data quality to derive a more reliable fraction of EHs with IR excess emission. IRAS data may also suffer from contamination by faint background sources, not visible on the DSS plates. Moreover, the fractional luminosity is rather sensitive to the wavelength at which the excess emission begins to be significant. Sylvester & Mannings (2000) estimate an uncertainty of about a factor of 2 in $L_{\rm IR}/L_*$ due to this effect, corresponding to the main source of uncertainty in our derivations.

The fractional dusty disk luminosity, $L_{\rm IR}/L_*$, follows the same trend as $F_{12,\rm obs}/F_{12,*}$ and $F_{25,\rm obs}/F_{25,*}$ (i.e., less for the ISO fluxes than for the IRAS data). HD 16141 shows the largest difference. We derived $L_{\rm IR}/L_* = 3.35 \times 10^{-4}$ from the ISO fluxes and 1.48×10^{-3} from the IRAS data for this star. The analyzed sample of EHs has an average difference of 2.5×10^{-4} for the fractional luminosity determinations based on the IRAS and the ISO fluxes. In spite of these differences, the IR excess emission exists independently of the used catalog.

The $L_{\rm IR}/L_*$ values derived for the EHs are a measure of the fraction of starlight which is absorbed and re-emitted by circumstellar dust, and hence indicate the optical depth of the disk material. The small values listed in Table 3 correspond to optically thin disks and are comparable to those obtained by Backman & Paresce (1993) for three well-known Vega-like stars. These authors calculate values between 10^{-5} and 10^{-3} for the fractional luminosities corresponding to β Pic, α Lyr and α PsA.

Figure 7 shows the histogram distributions of the fractional luminosities for the two samples of EHs analyzed: the

Table 3. Excess emission at 12 and 25 μm and fractional disk luminosity for the EHs sample.

Name	$F_{12,obs}/F_{12,*}$	$F_{25,obs}/F_{25,*}$	λ_{exc}	L_{IR}/L_*	Ref.	*FQUAL*	Variability
Class V objects							
HD 1237	1.78	1.34	12	1.99×10^{-4}	FSC	3211	SV
HD 3651	1.36	1.35	12	2.86×10^{-4}	FSC	3311	
HD 12661	1.55	3.44	12	4.59×10^{-4}	FSC	3111	
HD 17051	1.47	1.39	12	7.63×10^{-5}	FSC	3311	
HD 19994	1.81	1.66	12	1.42×10^{-4}	FSC	3311	MS, SV
			12	2.85×10^{-5}	ISO		
HD 23079	1.48	2.11	12	1.40×10^{-4}	FSC	3111	
HD 30177	1.71	5.09	12	9.49×10^{-4}	FSC	3111	
HD 41004A	2.38	6.57	12	3.64×10^{-3}	FSC	3111	
HD 50554	1.69	4.73	12	6.58×10^{-4}	FSC	3111	
HD 65216	2.30	3.05	12	1.34×10^{-3}	FSC	3111	
HD 89744	1.57	2.01	12	1.32×10^{-4}	FSC	3211	
HD 104985	2.03	1.93	12	6.35×10^{-4}	FSC	3311	
HD 106252	1.67	6.66	12	8.01×10^{-4}	FSC	3111	
HD 114729	1.92	2.83	12	3.21×10^{-4}	FSC	3111	S
HD 114762		7.78	25	1.48×10^{-3}	ISO		
HD 134987	1.53	2.87	12	3.42×10^{-4}	FSC	3111	
HD 141937	1.47	4.33	12	8.68×10^{-4}	FSC	3111	
HD 145675	1.40	1.22	12	3.09×10^{-5}	FSC	3311	
HD 147513	1.45	3.54	12	4.14×10^{-4}	PSC	3111	V
HD 169830	1.61	3.44	12	3.64×10^{-4}	PSC	3111	
HD 179949	1.66	3.38	12	3.76×10^{-4}	FSC	3211	
HD 192263	1.84	3.66	12	1.82×10^{-3}	FSC	3111	
HD 210277	1.98	5.54	12	9.06×10^{-4}	PSC	3111	
ϵ Eri	1.66	1.83	12	1.39×10^{-4}	FSC	3332	MS, V
GJ 86	1.91	1.54	12	1.86×10^{-4}	PSC	3311	SV
ρ CrB	1.62	1.57	12	9.09×10^{-5}	FSC	3311	MS
			25	1.15×10^{-4}	ISO		
τ Boo	1.67	1.66	12	7.36×10^{-5}	FSC	3311	V
		0.98	25	4.72×10^{-5}	ISO		
υ And	1.71	1.60	12	8.67×10^{-5}	FSC	3311	MS, SV
			60	6.36×10^{-6}	ISO		
16 Cyg	2.17	2.01	12	1.68×10^{-4}	FSC	3311	MS
47 UMa	1.78	1.39	12	5.59×10^{-5}	FSC	3311	SV
		0.96	25	8.14×10^{-5}	ISO		
51 Peg	1.63	1.49	12	9.31×10^{-6}	FSC	3311	SMS, SV
		1.09	25	7.65×10^{-5}	ISO		

class V luminosity stars and the evolved objects. The median of the groups are 3.32×10^{-4} and 2.09×10^{-4}, respectively. The KS statistical test indicates a high probability (~85%) of both distributions being identical.

We searched for a fractional luminosity, L_{IR}/L_*, trend with the age, plotting eight EHs with age determinations obtained from the literature (González 1999; González & Laws 2000; González et al. 2001; Suchkov & Schultz 2001; Chen et al. 2002). These authors used different methods to estimate the ages, such as evolutionary tracks or Ca II H, K core emission. We adopted the average when more than one determination was available for a given star. We found no clear trend. Large uncertainties in the age estimations may have prevented us, at least in part, from detecting a trend. In addition, our fractional luminosities are based on IRAS upper limits, introducing an additional uncertainty that may mask any correlation with age.

6.3. The criteria of Mannings & Barlow (1998)

Mannings & Barlow (1998) defined four criteria for selecting sources with IR excess among main sequence stars: 1) separation on the sky between IRAS and optical counterparts <60″; 2) IRAS fluxes quality "excellent" or "moderate"

Table 3. continued.

Name	$F_{12,obs}/F_{12,*}$	$F_{25,obs}/F_{25,*}$	λ_{exc}	L_{IR}/L_*	Ref.	*FQUAL*	Variability
Evolved objects							
HD 10697	1.81	1.99	12	1.40×10^{-4}	FSC	3111	
HD 16141	1.67	3.09	12	3.35×10^{-4}	FSC	3111	
HD 27442	1.59	1.41	60	1.79×10^{-6}	FSC	3331	MS, SV
HD 38529	1.62	2.06	12	2.35×10^{-3}	PSC	3111	
HD 39091	1.65	1.39	12	8.81×10^{-5}	FSC	3311	
HD 52265	1.60	3.96	12	5.35×10^{-4}	PSC	3111	C
HD 75289	1.82	4.80	12	3.59×10^{-3}	PSC	3111	
HD 130322	1.95	7.49	12	1.40×10^{-3}	FSC	3121	
HD 160691	1.64	1.92	12	1.12×10^{-4}	FSC	2311	
		1.07	25	1.23×10^{-4}	ISO		
HD 177830	1.65	2.82	12	9.09×10^{-4}	PSC	3111	
HD 178911	2.13	4.98	12	8.69×10^{-4}	FSC		MS, V
HD 190228	2.35	12.89	12	3.41×10^{-3}	PSC	3111	
HD 195019	1.79	1.95	12	4.54×10^{-4}	FSC	3211	MS
HD 213240	2.04	2.60	12	2.73×10^{-4}	FSC	3211	MS, SV
HD 216435	1.84	1.90	12	9.85×10^{-5}	FSC	3211	
HD 216437	1.59	1.53	12	1.08×10^{-4}	FSC	3311	
HD 217107	1.54	2.35	12	2.09×10^{-4}	FSC	3211	
Hip 75458	1.54	1.49	12	1.25×10^{-4}	FSC	3331	MS, SV
70 Vir	1.90	1.80	12	1.79×10^{-4}	FSC	3311	MS, V, C
			25	1.14×10^{-4}	ISO		
Unknown luminosity Class objects							
HD 20367	1.66	1.70	12	2.07×10^{-4}	FSC	3111	
HD 23596	1.67	3.76	12	6.36×10^{-4}	FSC	3111	
HD 28185	1.60	3.25	12	6.51×10^{-4}	FSC	3111	
HD 33636	1.91	2.85	12	3.27×10^{-4}	FSC	3111	
HD 40979	4.32	7.43	1.25	3.34×10^{-1}	FSC	3111	
			2.2	9.73×10^{-2}	FSC	3111	
HD 72659	1.49	3.90	12	4.59×10^{-4}	FSC	3111	
HD 74156	2.09	4.32	12	9.29×10^{-4}	FSC	3111	
HD 82943	1.51	2.41	12	2.07×10^{-4}	FSC	3211	
HD 128311	1.81	2.85	12	5.29×10^{-4}	FSC	3211	
HD 136118	1.64	6.86	12	8.69×10^{-4}	FSC	3111	
HD 150706	1.63	1.53	12	2.20×10^{-4}	FSC	3211	

Variability notes: MS: multiple system, SMS: suspected multiple system, V: variable star, SV: suspected variable, C: IRAS confusion or near-by star, S: at least one pixel saturation on DENIS *I*, *J*, *K* bands.

(i.e., *FQUAL* = 2 or 3, in Table 3); 3) luminosity class V; 4) IR excess satisfying at least one of the following inequalities,

$$\frac{\Delta_{12/25}}{\delta_{obs}} \equiv \frac{R_{12/25} - R^*_{12/25}}{\delta R_{12/25}} < -1 \quad (1)$$

$$\frac{\Delta_{25/60}}{\delta_{obs}} \equiv \frac{R_{25/60} - R^*_{25/60}}{\delta R_{25/60}} < -1 \quad (2)$$

where $R_{12/25} = F_{12}/F_{25}$ and $R_{25/60} = F_{25}/F_{60}$. R^* corresponds to the photospheric value calculated using the black-body function at the T_{eff} of the central object. $\delta R_{12/25}$ and $\delta R_{25/60}$ are expressions for the errors on the observed flux ratios (see Eqs. (3) and (4) in Mannings & Barlow 1998). If either or both inequalities (1) and (2) are satisfied then these authors claim that the observed flux densities significantly exceed those expected from a dust-free normal stellar photosphere.

Table 4 lists the quantities $\frac{\Delta_{12/25}}{\delta_{obs}}$ and $\frac{\Delta_{25/60}}{\delta_{obs}}$ for our sample of EHs. We initially restrict our analysis to the objects with luminosity class V and then relax criterion 3 of Mannings & Barlow (1998) to extend this analysis to evolved central stars and to objects of unknown luminosity class.

Of the 31 class V stars in our sample, 7 satisfy the criteria of Mannings & Barlow (1998) and have excesses above the photospheric level significantly greater than 3σ.

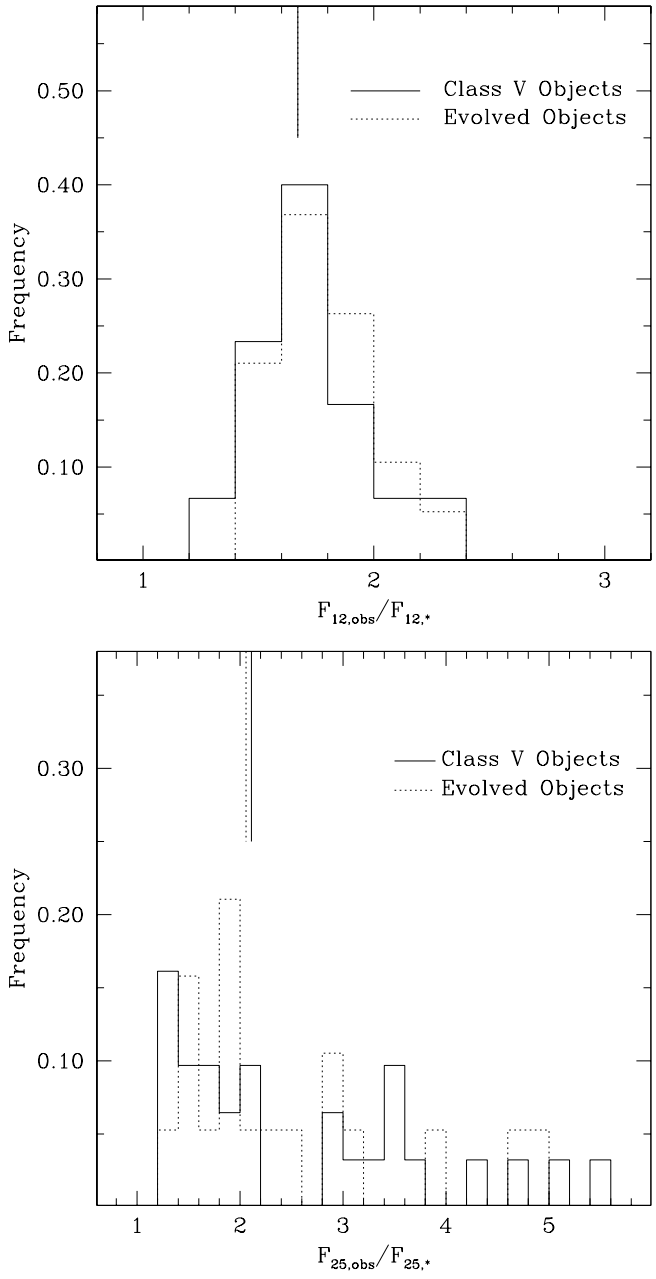

Fig. 5. $F_{12,\mathrm{obs}}/F_{12,*}$ (*upper panel*) and $F_{25,\mathrm{obs}}/F_{25,*}$ (lower panel) distributions for the class V (continuous line) and evolved (dotted line) EHs. We used IRAS data at 25 μm to construct the lower histogram except when only ISO photometry was available. The vertical line indicate the median of each distribution.

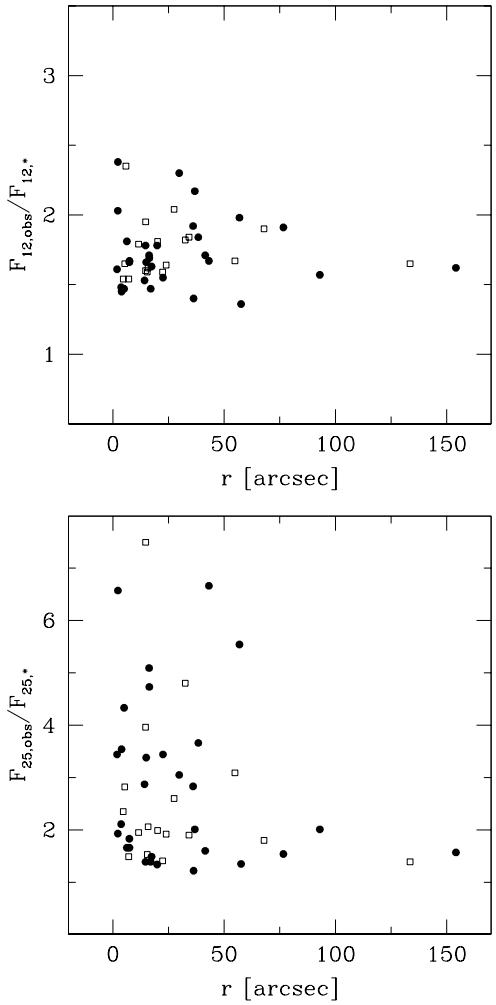

Fig. 6. Ratios of the observed to the photospheric fluxes at 12 and 25 μm vs. the difference between the optical and IRAS positions, r, in arcsec. Luminosity class V stars are represented by circles, evolved objects by open squares.

Mannings & Barlow (1998) suggested that only discrepancies between the observed and the expected flux density ratios greater than this limit (3σ) are meaningful. These objects are: HD 1237, HD 3651, HD 17051, HD 145675, HD 179949, ϵ Eri, and 47 UMa, representing 23% of the sample. We caution, however, that the photometric data used for 3 of these objects (HD 1237, ϵ Eri, and 47 UMa) may be uncertain due to possible variability (see Table 3). In the case of HD 1237 the only variability reported comes from the Hipparcos catalog and is quite small (<0.03 mag). For the other two objects, it is difficult to evaluate the quality of the used data. Including HD 1237, we consider that 6 out of 7 stars have reasonable good photometry, representing 19% of the luminosity class V EHs. Thus the criteria of Mannings & Barlow (1998) identify disks in 19 to 23% of the luminosity class V objects. The last percentage value includes ϵ Eri and 47 UMa.

Several objects in Fig. 3 are not selected by the criteria of Mannings & Barlow (1998). HD 41004A, HD 65216, HD 192263, and HD 210277 have poor quality IRAS fluxes (see Table 3). The star ρ CrB does not satisfy criterion 1, due to a large difference between the IRAS position and the optical counterpart (see Table 2). Although strictly speaking HD 104985 satisfies the four criteria of Mannings & Barlow (1998), the discrepancy between the observed and the expected flux ratios is less than 2σ. Following Mannings & Barlow (1998) we consider this difference not statistically significant.

Relaxing the luminosity class criterion we find that 6 out of 30 evolved or unknown luminosity class objects are selected according to the criteria of Mannings & Barlow (1998) (with a significance greater than 3σ in criterion 4), corresponding

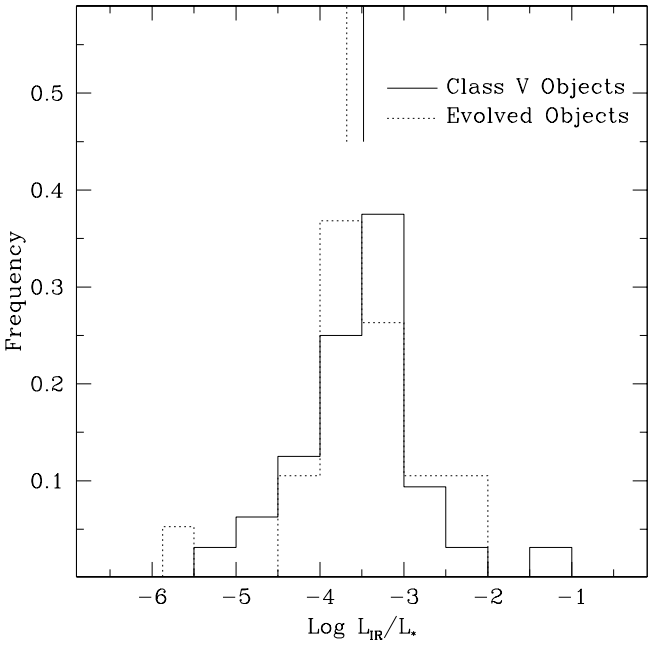

Fig. 7. Fractional dusty disk luminosity distributions for the class V (continuous line) and the evolved (dotted line) EHs. We used IRAS data to construct the histograms in this figure except when only ISO photometry was available. The medians of both distributions are indicated in the upper part of the diagram.

to 20% of the sample. These objects are: HD 21647, HD 82943, HD 128311, HD 150706, HD 160691 and HD 217107 (see Fig. 4).

Five of the EHs have been previously announced to have circumstellar disks. These stars are: HD 17051, HD 210277, ϵ Eri, ρ CrB and 55 Cnc. Pantin et al. (2000) obtained coronographic images of HD 17051 and Trilling et al. (2000) of HD 210277, ρ CrB and 55 Cnc. Dominik et al. (1998), using ISO data, reported the detection of excess emission at 60 μm in 55 Cnc. However, Schneider et al. (2001) and Jayawardhana et al. (2002) failed to find evidence of the presence of circumstellar material around 55 Cnc based on high sensitivity near-IR and sub-millimeter data. Schneider et al. (2001) should have been able to detect fluxes to a level 10 times lower than the disk reported by Trilling et al. (2000). Jayawardhana et al. (2002) suggested the background nature of the 60 μm emission associated with 55 Cnc based on the non-circumstellar characteristic of the 3 peaks detected at 850 μm, 40–60″ away from the star. This result casts some doubts on the true circumstellar nature of the IR excess associated with this group of objects except for ϵ Eri for which the presence of a dusty disk seems to be well established. Greaves et al. (1998) have obtained images at 850 μm of this star detecting a ring of dust, peaking at a distance of 60 AU from the central star.

The criteria of Mannings & Barlow (1998) select two of these objects (HD 17051 and ϵ Eri), assuming that the uncertainty in photometric data is negligible. These criteria fail to identify HD 210277 and ρ CrB for the reasons explained above (i.e., IRAS data quality and positional association, respectively). 55 Cnc is not analyzed, as mentioned above.

7. Polarimetry of the EHs

We used the Leroy (1993) and Heiles (2000) catalogs to compile optical polarimetry data for 26 of the EHs. To compare the polarimetry properties of the EH group with the Vega-like objects we collected similar information on 44 objects from the literature (Bhatt & Manoj 2000; Oudmaijer et al. 2001). We selected near-by Vega-like candidate objects with $d < 100$ pc. Most of these stars are located off the galactic plane. The average galactic latitude of this sample is ∼43° and only one star (HD 139664) has $|b| \sim 8.5°$. Within this range of distance and relatively high galactic latitude, the interstellar polarization is ∼0.1% (Reiz & Franco 1998; Bhatt & Manoj 2000). In the case of the EHs, the sample of the 26 compiled objects lies between 3 and 42 pc and thus we expect the interstellar contribution to the measured polarization be small.

Figure 8 shows the histogram distributions for the EH and Vega-like groups. Yudin (2000) analyzed the polarization distributions for 174 T Tauri and 149 Herbig AeBe stars (see Figs. 7 and 8 in Yudin 2000). Table 5 lists the medians corresponding to each distribution.

Most of the EHs have very low polarization values, comparable in some cases to their uncertainties. Some interstellar contribution is likely but not significant as most of the objects have essentially $p \sim 0$. In addition, as discussed in Sect. 5, no significant reddening in $(B - V)$ was derived for the group of EHs, suggesting that the amount of interstellar matter is neglectable.

The largest optical polarization values correspond to HD 114762 and HD 179949 with a polarization of 0.090% and 0.080%, respectively. HD 114762 has a large flux excess and fractional luminosity at 25 μm (see Table 3). The criteria of Mannings & Barlow (1998) are not applied to this object as no IRAS data are available. However, the corresponding SED (see Fig. 3) shows significant IR excess at wavelengths longer than 25 μm. HD 179949 satisfies the criteria of Mannings & Barlow (1998). The SED in Fig. 3 shows significant IR excess. The flux ratios, $F_{12,\mathrm{obs}}/F_{12,*}$ and $F_{25,\mathrm{obs}}/F_{15,*}$, and the fractional luminosity, L_{IR}/L_*, in Table 3 are close to or higher than the median value for the group of the class V EHs. The excess infrared emission for these two objects suggest that the measured polarizations are probably mostly circumstellar rather than interstellar.

The median polarization for EHs is almost identical to that for Vega-like objects (see Table 5). However, the KS test indicates that the corresponding histograms are significantly different at the 98% confidence level. Although most Vega-like objects have very low polarization values, a significant fraction of the compiled sample (∼30%, 13 out 44) shows degrees of polarization in excess of ∼0.1% interstellar contribution, suggesting the presence of circumstellar dust (see also Bhatt & Manoj 2000). In fact, the statistical difference between the two distributions is mainly due this relatively high polarization extension of the Vega-like distribution. Circumstellar dust around Vega-like stars can scatter and thus polarize the light from the central star.

For objects with $p < 0.1\%$ it is difficult to disentangle the interstellar and the circumstellar components. However,

Table 4. Criteria of Mannings & Barlow (1998) for the EHs.

Name	$\frac{\Delta_{12/25}}{\delta_{\rm obs}}$	$\frac{\Delta_{25/60}}{\delta_{\rm obs}}$	Criteria of Mannings & Barlow (1998)
Luminosity Class V objects			
HD 1237	1.24	−14.67	Y
HD 3651	0.02	−4.12	Y
HD 12661	−4.48	−15.32	N
HD 17051	0.56	−8.81	Y
HD 19994	0.42	−8.93	N
HD 23079	−1.74	−23.61	N
HD 30177	−7.78	−18.95	N
HD 41004A	−7.17	−45.6	N
HD 50554	−6.82	−13.03	N
HD 65216	−1.7	−56.8	N
HD 89744	−1.74	−10.43	N
HD 104985	0.57	−1.65	N
HD 106252	−9.70	−3.58	N
HD 114729	−1.53	−17.06	N
HD 134987	−3.31	−6.97	N
HD 141937	−7.98	−41.14	N
HD 145675	0.90	−9.66	Y
HD 147513	−6.89	−15.84	N
HD 169830	−4.23	−22.50	N
HD 179949	−3.54	−11.68	Y
HD 192263	−3.66	−22.36	N
HD 210277	−8.19	−16.71	N
ϵ Eri	−1.40	−31.15	Y
GJ 86	1.41	−7.51	N
ρ CrB	0.33	−6.88	Y
τ Boo	0.04	−0.16	N
υ And	0.70	−2.06	N
16 Cyg	0.82	−15.98	N
47 UMa	2.09	−5.46	Y
51 Peg	0.62	−12.07	N
Evolved objects			
HD 10697	−0.32	−6.82	N
HD 16141	−3.31	−6.70	N
HD 27442	2.29	1.14	N

Tamburini et al. (2002) analyzed the optical polarimetry properties of the same group of EHs in relation to a group of nearby stars not known to have planets and found that the distributions are different. The EH polarization distribution peaks at very small values (close to $p \sim 0.0\%$). These authors also noticed that the degree of polarization for the EHs is not strictly correlated with the presence of a planet or planets. However, the polarization correlates with the orbital eccentricity of the system. EHs with planets with highly eccentric orbits tend to have low polarizations. Low eccentricity systems, on the other hand, have high polarizations.

The T Tauri and Herbig AeBe groups have median polarizations (1.0% and 1.5%, respectively) that are significantly larger than those for the Vega-like objects (0.05%) and the EHs (0.02%). This difference may indicate that the relatively hot dust (producing the polarization at optical wavelengths) is being depleted with time. T Tauri and Herbig AeBe objects have ages of $\sim$1–10 $\times$ 10^6 yr, while Vega-like stars and EHs are older, with ages of $\sim$1–10 $\times$ 10^8 yr.

In Fig. 9 we plot the percentage of polarization vs. the derived fractional luminosity, $L_{\rm IR}/L_*$, for the sample of EHs. No clear trend is evident in this figure. The two groups (class V and evolved objects) are well mixed on this plot. This sample includes ϵ Eri which is associated with an almost pole-on circumstellar disk (Greaves et al. 1998) and has a relatively small degree of polarization (0.007%). The fact that the disk almost coincides with the plane of the sky explains the low value of polarization for this object.

8. Summary and discussion

We have collected optical and IR photometry for a group of 61 EHs. The color–color diagram, $K_{\rm s}$ − [12] vs. $J - K_{\rm s}$, of this

Table 4. continued.

Name	$\frac{\Delta_{12/25}}{\delta_{obs}}$	$\frac{\Delta_{25/60}}{\delta_{obs}}$	Criteria of Mannings & Barlow (1998)
Evolved objects			
HD 38529	−1.28	−179.69	N
HD 39091	1.74	−49.83	N
HD 52265	−5.51	−26.34	N
HD 75289	−7.32	−135.18	N
HD 130322	−9.93	−15.32	N
HD 160691	−1.09	−10.93	Y
HD 177830	−3.25	−26.05	N
HD 178911	−4.73	−26.30	N
HD 190228	−18.35	−21.19	N
HD 195019	−0.28	−31.07	N
HD 213240	−0.97	−15.50	N
HD 216435	−0.13	−10.27	N
HD 216437	0.25	−12.65	Y
HD 217107	−1.95	−7.96	Y
Hip 75458	0.61	2.06	N
70 Vir	0.46	−0.65	N
Unknown luminosity Class objects			
HD 20367	−0.09	−30.91	N
HD 23596	−6.35	−37.28	N
HD 28185	−4.52	−38.42	N
HD 33636	−1.83	−15.90	N
HD 40979	−2.69	−16.50	N
HD 72659	−5.50	−11.87	N
HD 74156	−3.72	−33.33	N
HD 82943	−2.35	−16.09	Y
HD 128311	−2.44	−9.07	Y
HD 136118	−11.66	−12.55	N
HD 150706	0.27	−45.48	Y

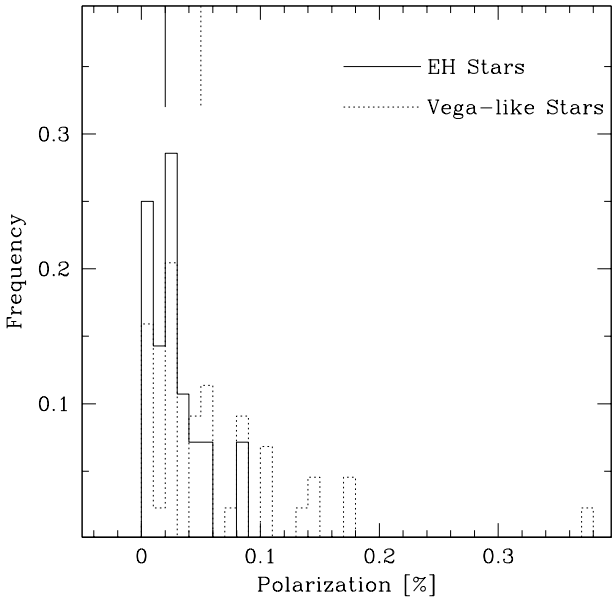

Fig. 8. Polarization distributions for the EH (thick line) and Vega-like (dotted line) stars. The median of each distribution is indicated.

sample shows a clear 12 μm excess with respect to the main sequence stars (devoid of significant amounts of circumstellar material) and roughly comparable to Vega-like stars. The medians of the $K_s - [12]$ distributions are: ∼0 for normal main sequence stars, 0.5 for Vega-like objects (Fajardo-Acosta et al. 2000), and 0.38 for the analyzed EH sample. The $K_s - [25]$ vs. $J - K_s$ color–color plot of the EH group also indicates 25 μm excess.

We have constructed the spectral energy distributions of 61 EHs combining photometry from different surveys. The black-body model reproduces the observed spectral distributions between 0.43 and 12 μm quite satisfactorily for most of the objects. However, most of the stars in our sample show IR excess emission at $\lambda \gtrsim 12$ μm that cannot be fitted by a single black-body model and thus cannot be attributed to the photospheric contribution. Whereas no significant near-IR excess is evident or expected in these stars, excess in the mid- or far-IR may be significant.

We have applied different indicators, previously used in the literature to select Vega-like candidates among main sequence stars, to better quantify mid- or far-IR excesses in the analyzed

Table 5. Median polarization values.

Group	No. of objects	Median polarization %	Reference
EH	26	0.02	Leroy (1993), Heiles (2000)
Vega-like	44	0.05	Yudin (2000), Bhatt & Manoj (2000), Oudmaijer et al. (2001)
T Tauri	174	1.0	Yudin (2000)
Herbig AeBe	149	1.5	Yudin (2000)

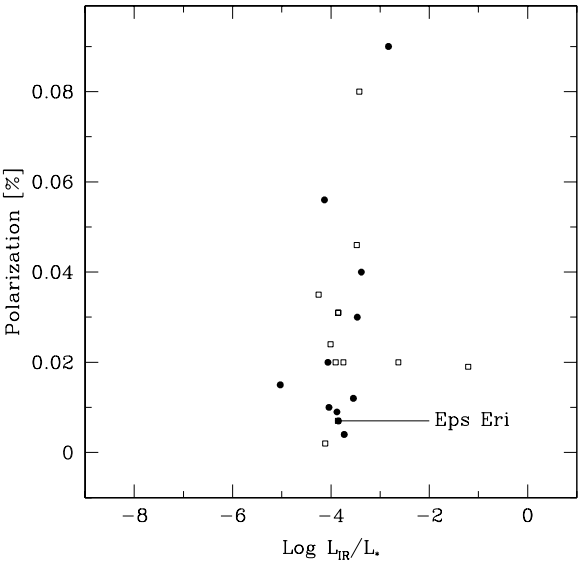

Fig. 9. Percentage of polarization vs. Log L_{IR}/L_* for the sample of EHs. The circles indicate class V objects and the open squares evolved stars. The position of ϵ Eri (associated with an almost pole-on dusty circumstellar disk; Greaves et al. 1998) is indicated.

EH sample. In particular, we have used the photospheric flux excesses at 12 and 25 μm ($F_{12,obs}/F_{12,*}$ and $F_{25,obs}/F_{25,*}$), the fractional dusty disk luminosity (L_{IR}/L_*), and the density flux ratios ($R_{12/25}$ and $R_{25/60}$) in combination with positional associations and IRAS data quality constraints of Mannings & Barlow (1998).

Whereas the photospheric fluxes at 12 and 25 μm and the fractional dusty disk luminosity indicate that as a group the EHs have an excess with respect to the photospheric level no constraints on IRAS data quality or positional association are applied. On the other hand, the criteria of Mannings & Barlow (1998) establish additional restrictions on data quality and source positional correspondences, allowing us to derive a more reliable fraction of objects with disk among the EHs. These criteria identify disks in 19–23% (i.e., in 6–7 out of 31) of the class V and in 20% (i.e., in 6 out of 30) of the evolved EHs. For all these objects the difference between the observed and the expected density flux ratios is significantly greater than 3σ.

Several searches for Vega-like systems estimate a similar fraction of objects with IR excess emission among main sequence stars (i.e., ∼15% Sylvester et al. 2001; Fajardo-Acosta et al. 2000). This excess emission is likely due to the presence of circumstellar dust. However, in view of the poor spatial resolution and confusion problems of IRAS, higher resolution and sensitivity data are required to confirm the circumstellar nature of the detected emissions.

We have collected optical polarization for 26 EHs from the literature. These objects have very modest degrees of polarization with a median of 0.02% and comparable to Vega-like stars (0.05%). Both groups have significant lower median optical polarization values than T Tauri (1.0%) and Herbig AeBe (1.5%) stars. However, we failed to find a trend in the fractional dusty disk luminosity, L_{IR}/L_*, vs. the degree of polarization for the analyzed sub-sample of 26 EHs. Similarly, no clear correlation is apparent from the comparison with the fractional dusty disk luminosity, L_{IR}/L_*, and with the age of eight EHs taken from the literature.

Acknowledgements. This research has made use of the SIMBAD database, operated at CDS, Strasbourg, France. 2MASS and DENIS data were employed in this analysis. An anonymous referee suggested a revision of our statistics on EH stars with excess emission that stressed the significance of the results.

References

Allende Prieto, C., & Lambert, D. L. 1999, A&A, 352, 555
Augereau, J. C., Lagrange, A. M., Mouillet, D., & Menard, F. 1999, A&A, 350, L51
Aumann, H. H., Beichman, C. A., Gillett, F. C., et al. 1984, ApJ, 278, L23
Backman, D. E., & Paresce, F. 1993, in Protostars and Planets III, ed. E. H. Levy, J. I. Lunine, & M. S. Mathews (Tucson: Univ. Arizona Press), 1253
Bessel, M. S. 1979, PASP, 91, 589
Bessel, M. S., & Brett, J. M. 1988, PASP, 100, 1134
Bhatt, H. C., & Manoj, P. 2000, A&A, 362, 978
Butler, R. P., Marcy, G. W., Williams, E., et al. 1996, PASP, 108, 500
Chen, Y. Q., & Zhao, G. 2002, ChJAA, 2, 151
Cohen, M., Wheaton, W. A., & Megeath, S. T. 2003, AJ, 126, 1090
Cutri, R. M., Skrutskie, M. F., van Dyk, S., et al. 2003, CDS Online Catalog II/246
Dominik, C., Laureijs, R. J., Jourdain de Muizon, M., & Habing, H. J. 1998, A&A, 329, L53
Egan, M. P., Price, S. D., Moshir, M. M., et al. 1999, CDS online catalog V/107
Fajardo-Acosta, M. B., Beichman, C. A., & Cutri, R. M. 2000, ApJ, 538, L155
Fouqué, P., Chevallier, L., Cohen, M., et al. 2000, A&AS, 141, 313
Golderich, P., & Sari, R. 2003, ApJ, 585, 1024
González, G. 1999, MNRAS, 308, 447
González, G., & Laws, C. 2000, AJ, 119, 390
González, G., Laws, C., Tyagi, S., & Reddy, B. E. 2001, AJ, 121, 432

Greaves, J. S., Holland, W. S., Moriarty-Schieven, G., et al. 1998, ApJ, 506, L133
Heiles, C. 2000, AJ, 119, 923
IRAS Catalogs and atlases explanatory supplement, 1988, ed. C. Beichman, G. Neugebauer, H. J. Habing, P. E. Clegg, & T. J. Chester (Washington, DC: GPO), NASA RP-1190, vol. 1
Jayawardhana, R., Holland, W. S., Kalas, P., et al. 2002, ApJ, 570, L93
Jura, M. 1999, ApJ, 515, 706
Kalas, P., Graham, J., Beckwith, S. V. W., et al. 2002, ApJ, 567, 999
Kenyon, S., & Hartmann, L. 1995, ApJS, 101, 117
Kessler, M. F., Steinz, J. A., Anderegg, M. E., et al. 1996, A&A, 315, L27
Kholopov, P. N., Samus, N. N., Frolov, M. S., et al. 1998, A combined general catalog of variable stars, edition 4.1, Moscow, ed., Precision Photometry: Astrophysics of the Galaxy (Schenectady: L. Davis Press), 27
Laureijs, R. J., Jourdain de Muizon, M., Leech, K., et al. 2002, A&A, 387, 285
Leroy, J. L. 1993, A&AS, 101, 551
Levison, H. E., Lissauer, J. J., & Duncan, M. J. 1998, AJ, 116, 1998
Lin, D. N. C., Bodenheimer, P., & Richardson, D. C. 1996, Nature, 380, 606
Malfait, K., Bogaert, E., & Waelkens, C. 1998, A&A, 331, 211
Mannings, V., & Barlow, M. 1998, ApJ, 497, 330
Marcy, G. W., & Butler, R. P. 1996, ApJ, 464, L147
Moshir, M., Copan, G., Conrow, T., et al. 1989, Explanatory supplement to the IRAS faint source survey, version 2 (JPL D-10015 8/92; Pasadena: JPL) (FSC)
Noyes, R. W., Saurabh, J., Korzennik, S. G., et al. 1997, ApJ, 483, 111
Oudmaijer, R. D., Palacios, J., Eiroa, C., et al. 2001, A&A, 379, 564
Pantin, E., Els, S., Marchis, F., et al. 2000, BAAS, 32, 1646
Press, W. H., Teukolsky, S. A., Vetterling, W. T., & Flannery, B. P. 1992, Numerical recipes in Fortran: The art of scientific computing (Cambridge University Press), 2nd edition, 617
Reid, N. 2002, PASP, 114, 306
Reiz, A., & Franco, G. A. P. 1998, A&AS, 130, 133
Schmidt-Kaler, Th. 1982, in Landolt-Bornstein, Numerical data and functional relationships in science and technology, Group VI, Astronomy, Astrophysics and Space Research, ed. K. Shaifers, & H. H. Voigt, 2b (Berlin: Springer Verlag), 14
Schneider, G., Smith, B. A., Becklin, E. E., et al. 1999, ApJ, 513, L127
Schneider, G., Becklin, E. E., Smith, B. A., et al. 2001, ApJ, 121, 525
Song, I., Caillault, J. -P., Barrado y Navascués, D., et al. 2000, ApJ, 532, L41
Song, I., Caillault, J.-P., Barrado y Navascués, D., & Stauffer, J. R. 2001, ApJ, 546, 352
Suchkov, A. A., & Schultz, A. B. 2001, ApJ, 549, L237
Sylvester, R. J., & Mannings, V. 2000, MNRAS, 313, 73
Sylvester, R. J., Skinner, C. J., Barlow, M. J., & Mannings, V. 1996, MNRAS, 279, 915
Sylvester, R. J., Dunkin, S. K., & Barlow, M. J. 2001, MNRAS, 327, 133
Tamburini, F., Ortolani, S., & Bianchini, A. 2002, A&A, 394, 675
Thé, P. S., de Winter, D., & Perez, M. R. 1994, A&AS, 104, 315
Trilling, D. E., Brown, R. H., & Rivkin, A. S. 2000, ApJ, 529, 499
Vogt, S. S., Marcy, G. W., Butler, R. P., & Apps, K. 2000, ApJ, 536, 902
Weinberger, A. J., Becklin, E. E., Schneider, G., et al. 1999, ApJ, 525, L53
Yudin, R. V. 2000, A&AS, 144, 285
Zuckerman, B. 2001, ARA&A, 39, 549